

Partial hydrogenation of soybean oil using metal decorated integral-asymmetric polymer membranes: effects of morphology and membrane properties

Journal of Membrane Science 348(1-2) 99-108, 2010

D. Singh, M. E. Rezac*, P. H. Pfromm

Department of Chemical Engineering, Kansas State University, 1005 Durland Hall, Manhattan, Kansas, 66506-5102, USA

Abstract

Three phase reaction schemes pose numerous challenges to reactor design due to the slow diffusional mass transfer of reactants from the gas phase through a liquid to the active sites of the catalyst. An example is partial hydrogenation of vegetable oil which is traditionally carried out in a batch autoclave by bubbling hydrogen gas through a slurry of oil and solid catalyst particles containing Ni. Unwanted trans fatty acids (TFA) are formed during this process due to the scarcity of hydrogen at the active catalyst sites. Here we investigate the use of metal decorated integral-asymmetric polymer membranes to enable the supply of dissolved hydrogen near the location where the liquid oil phase contacts the catalyst. Hydrogen gas is supplied to the porous sub-structure of the asymmetric membrane where it dissolves in the thin skin layer of the membrane and emerges as dissolved hydrogen on the metal-decorated side of the membrane where the oil is present. Temperature and pressure are compatible with existing facilities. All membranes produced low TFA (2.6-4.6 wt% at Iodine Value of 95) compared to the slurry process. A 1000 metric ton per day soybean oil hydrogenation facility would require 2-3000 m² membrane area with a total of 90 grams of Pt metal catalyst. This could be envisioned as metal sputtered hollow fibers packaged in conventional modules.

*: to whom correspondence shall be addressed, e-mail rezac@ksu.edu, phone 785-532-5584, fax 785-532-7372

1 Introduction

Reactions involving a liquid, a solid catalyst, and a reactant that is gaseous at reaction conditions pose many challenges to reactor design, one of them being the slow mass transfer of reactants from a gas phase through a liquid to the active catalyst sites. This liquid-phase mass transfer resistance frequently causes a scarcity of one or more of the reactants at the catalyst surface. This may lead to lower reaction rates and in some cases have a detrimental effect on the composition of the final product. The situation is exacerbated if the liquid phase is viscous and/or has a low solubility for the gas phase reactant as is the case with hydrogen and vegetable oil.

Partial hydrogenation of vegetable oils is an important reaction in the food industry, used for the production of base stocks for margarines and shortenings. In the U.S. alone, the annual production of margarines and shortenings was around 8 billion pounds in 2007[1]. The traditional approach to hydrogenation of vegetable oil is bubbling hydrogen through oil in a stirred batch autoclave and hydrogenating over a nickel based catalyst that is supported on particles suspended in the oil. This slurry reactor approach leads to the formation of relatively high amounts of TFA [2; 3] generally attributed to low availability of hydrogen at the catalyst due to significant hydrogen mass transfer limitations in the oil phase [4].

In this paper, we study metal-decorated integral-asymmetric polymer membranes for partial hydrogenation of vegetable oil. The concept is to alleviate hydrogen starvation of the catalyst surface by supplying dissolved hydrogen near or at the catalytic sites. This should promote the desired hydrogenation and reduce the undesirable TFA formation based on the literature on catalyzed hydrogenation of oils. After initial successful proof-of-concept of the process at pressures and temperatures compatible with the existing hydrogenation processes [5] we focus

here on the membrane morphology and the impact of the membrane properties on the hydrogenation results.

2 Background

2.1 Molecular architecture of vegetable oil

Vegetable oils are mixtures of triglycerides which consist of one molecule of glycerol combined with three molecules of fatty acid residues. The major fatty acids present are palmitic acid (C16:0, nomenclature: 16 carbon atoms with zero double bonds), stearic acid (C18:0, m.p. 70°C), oleic acid (C18:1), linoleic acid (C18:2), linolenic acid (C18:3, m.p. -13°C), and minor amounts of other fatty acids (C14:0 to C24:0). It is the composition of the major fatty acids that determines the bulk physical and chemical properties of fats and oils. The melting characteristics and oxidative stability depend on the fatty acid residues attached to the glycerol backbone. The oxidative stability of different fatty acids follows the order: C18:1 > C18:2 > C18:3. A triglyceride with one stearic and two oleic acid residues is 15 times more oxidatively stable than a triglyceride with three linoleic acids [6].

2.2 Vegetable oil hydrogenation

Hydrogenation involves adding hydrogen to double bonds of fatty acids present in vegetable oil to obtain a fatty acid composition profile that has a high oxidative stability and a melting point most suited for a particular application. The main goals are to minimize C18:3 because of its poor oxidative stability while maintaining C18:2 since it forms a valuable part of the human diet, and minimizing the formation of saturated C18:0. Recent health concerns regarding TFA [7; 8] have added avoiding TFA formation to the list of requirements for vegetable oil hydrogenation.

The conventional hydrogenation of vegetable oil is carried out in a stirred batch autoclave (typically 30,000-90,000 pounds of oil [11]) over nickel based catalyst in a slurry at 110-190°C, 30-70 psi hydrogen pressure, with 0.01-0.15wt% Ni catalyst [9] (supported on Kieselguhr, silica-alumina, or carbon[10]). This approach (Figure 1a) relies on the dissolution of hydrogen in the oil followed by convective (supported by stirring) and diffusive (in the particle boundary layer) hydrogen transport to the catalytic sites. The various reactions occurring during hydrogenation of vegetable oil can be described by the Horiuti-Polanyi mechanism [4; 12]. The hydrogen diffuses through the liquid oil and is adsorbed on the catalyst surface where it dissociates into two adsorbed hydrogen atoms which react with the adsorbed fatty acid molecule to form an unstable half-hydrogenated intermediate. Depending on the concentration of hydrogen at the catalyst surface, this intermediate complex can gain a hydrogen atom and thereby hydrogenate or lose a hydrogen atom and in the process may isomerize. Figure 1 shows the hydrogenation and isomerization reactions of linolenic fatty acid (C18:2) to oleic acid (C18:1) [4]. Details about hydrogenation kinetics are available elsewhere [13; 14; 15].

The overall hydrogenation rate depends strongly on the concentration of hydrogen in the bulk oil [4]. However, the low solubility of hydrogen in oils leads to hydrogen starvation of the catalytic sites and promotes isomerization to TFA. Decreased temperature, increased agitation, and increased hydrogen pressure reduce detrimental hydrogen mass transfer limitations [3; 16]. However, the reaction conditions must be kept in an operating window that does not render the process uneconomical. Excessive hydrogen pressure, for example, could only be used at considerable capital expense.

2.3 *Published novel catalytic membrane approaches*

Recent studies [17; 18; 19; 20] report novel reactor designs for hydrogenation of vegetable oils to maximize the delivery of hydrogen to the catalyst surface and minimize TFA production. Most of these studies [17; 19; 20] use porous membranes as gas-liquid-solid contactors to alleviate mass transfer issues

Schmidt and Schomacker [19] describe the development of a porous membrane with catalyst particles on the surface (Figure 2b). A mixture of oil and gaseous hydrogen is pumped through the pores [19]. The mass-transfer limitations were hoped to be reduced. However, the TFA generated in this system was unfortunately higher than that achieved in the conventional system [19].

An alternative approach (Figure 2c) employed a porous membrane used in "diffuser mode" with catalyst deposited on a part of the pore walls and oil filling that part of the pore. Veldsink et al. [20] used porous zirconia membranes (20 nm pore size) and Pd catalyst impregnated on the pore walls. The aim was to increase the hydrogenation selectivity by eliminating intraparticle diffusion limitations. High selectivities were obtained for the hydrogenation of polyunsaturated triglycerides to produce mono-saturated products yet this also produced very high levels of TFA [20].

In an attempt to overcome the hydrogen supply limitations, an electrochemical process (Figure 2d) for the hydrogenation of vegetable oil has been devised [17; 21; 22; 23]. Oxygen and hydrogen are generated by splitting water electrochemically. The hydrogen is evolved at a cathode that also contacts the oil and acts as the hydrogenation catalyst. The oxygen is a byproduct. This approach produced very low TFA level. This approach essentially replaces the hydrogen production via water gas shift reaction from natural gas with electrochemically

produced hydrogen. Economics of the process compared to the traditional approach and our approach will be discussed below.

2.4 Approach employed here

We have devised an approach taking advantage of the high gas transport rates of integral-asymmetric polymeric membranes with essentially perfect non-porous ultrathin skins (about <1 micrometer effective skin thickness), but using the membrane "reversed" by applying hydrogen to the porous substructure of the membrane while liquid oil is present on the skin side (Figure 2e). Hydrogen molecules dissolve in the skin layer and diffuse towards the "oil" side under the partial pressure driving force created by essentially pure hydrogen on the substructure side and hydrogen consumption by hydrogenation on the oil side. The hydrogen transport rate can be adjusted through the partial pressure driving force that is applied. The hydrogen transport rate is self-regulating since the partial pressure of hydrogen in the oil phase increases if hydrogen is not consumed, which reduces the driving force for hydrogen transport. Hydrogen is essentially supplied to the catalyst "on demand" with the maximum rate of supply limited only by the hydrogen pressure and the membrane characteristics. In fact, the process is operated with a hydrostatic oil pressure exceeding the hydrostatic pressure of the hydrogen.

The ultrathin tight polymer membrane skin layer effectively excludes convective gas transport from the hydrogen side into the oil via bubbles. Gas transport in the skin is by solution-diffusion. Similarly, no oil can leak into the substructure of the membrane which would impede hydrogen transport and cause process upsets.

The membrane skin decouples the oil side hydraulically from the gas side allowing largely independent control of the hydrostatic pressure difference (and oil flow rate) from the hydrogen driving force and thereby hydrogen flux. A porous membrane on the other hand requires finely

tuned control of hydrostatic pressure differences to avoid oil or gas intrusion and/or blow out for the membrane pores.

The smooth skin of integral asymmetric membranes provides a good support for uniform metal deposition with high surface-to-volume ratio. Any surface features might lead to uneven metal deposition and/or mass transfer obstacles.

3 Experimental

3.1 Materials

Soybean oil (Iodine Value IV = 129-131) was purchased from MP Biomedicals (Solon, OH). The composition of soybean oil as measured in our laboratory is (reported as weight percent): C16:0, 11.6-12.0; C18:0, 4.3-4.4; C18:1, 21.6-23.8; C18:2, 51.6-53.3; C18:3, 7.1-7.8; total trans fatty acids, 0.7-1.2; C18:1 trans, 0.0; C14:0-C24:0, 0.9-1.5. Polyetherimide (PEI, Ultem-1000) to cast the integral-asymmetric membranes was purchased from General Electric (Huntersville, NC). Acetic acid (HPLC grade), acetone (99.5%), p-xylene (99.9%), and dichloromethane (99.9%), were from Fisher Scientific (Rochester, NY), 1,1,2,2-tetrachloroethane (98%) was from Sigma Aldrich (St. Louis, MO). The platinum (Pt) sputter target (99.95wt% Pt) was from Ted Pella Inc. (Redding, CA). Ultra high purity hydrogen (min. 99.999%) and nitrogen (min. 99.999%) were obtained from Linweld Inc. (Lincoln, NE).

3.2 Membrane preparation and testing

Integral asymmetric polyetherimide (PEI) membranes were fabricated using the phase inversion process as described elsewhere [24]. A 15.9 wt% solution of PEI was prepared in a mixture of solvents (dichloromethane 54.6wt%; 1,1,2,2-tetrachloroethane 4.8wt%) and pore forming agents (xylene 17.6wt%; acetic acid 7.1wt%). The polymer solution was cast on a cooled glass plate (11x8.5 inch, 16-18°C) using a Gardner knife set to a gap of about 350

micrometers (μm). The knife gap establishes the thickness of the polymer solution layer but the enormous success of asymmetric membranes is based on the about three orders of magnitude thinner (compared to the final total membrane thickness) selective skin layer formed during phase inversion. After 3 seconds of air drying the glass plate carrying the polymer solution layer was immersed in acetone ($12\text{-}16^\circ\text{C}$, 30 minutes). The nascent membrane floats off the glass plate and is then air dried overnight. The membranes thus formed are integral-asymmetric membranes with a dense skin of thickness of about $0.1\text{-}0.5\ \mu\text{m}$ and a porous substructure $100\text{-}160\ \mu\text{m}$ thick. Figure 3 shows a scanning electron micrograph (SEM) and transmission electron micrograph (TEM) of a cross-section of an integral-asymmetric PEI membrane. The expected highly porous substructure and thin dense skin can be seen. It should be noted that we designate the membrane skin layers as ultrathin based on the fact that essentially perfect sub-micron effective skin layer thicknesses are obtained (as tested by comparison to thick film hydrogen/nitrogen selectivities). This is an example of a perfect nano-scale material (thickness down to on the order of 100 nanometer) produced on a macroscopic scale.

Circular stamps 4.7 cm in diameter were cut from the membrane sheets and tested in a filter holder (model XX4404700, Millipore Corp., Billerica, MA) for their gas fluxes (hydrogen and nitrogen) using a constant-volume variable-pressure apparatus (similar to the one described elsewhere [25]) at 25°C and 50 psig. The normalized gas fluxes in GPU (Gas Permeation Unit, $1\ \text{GPU} = 10^{-6}\ \text{cm}^3(\text{STP})\ \text{cm}^{-2}\ \text{s}^{-1}\ \text{cm}\ \text{Hg}^{-1}$) were measured and the ideal gas selectivity $\alpha_{\text{H}_2/\text{N}_2}$ was calculated as the ratio of the normalized single gas fluxes. Thick films of PEI have been measured and show $\alpha_{\text{H}_2/\text{N}_2}$ of about 181 at 25°C [26; 27].

Pt was applied to the membrane skin by sputtering (using DESK II magnetron sputter, Denton Vacuum, Moorestown, NJ, 3-9 seconds at 45 mA, 100 mtorr) before using the membrane

for hydrogenation run. Sputtered membranes were re-tested for their gas fluxes and ideal gas selectivities for quality control. In most cases the gas flux of the membranes was reduced after sputtering as can be expected due to the relatively nonpermeable nature of the metal. Hydrogen permeation through Pt is negligible when compared to the gas transport through PEI at temperatures below 80 °C [28].

The Pt loading on the membrane was estimated by sputtering Pt on a quartz crystal for 3, 6, and 9 seconds and measuring the weight change (Table 1) using a quartz crystal microbalance (QCM, model RQCM, Maxtek Inc., East Syracuse, New York). The Pt loading increased fairly linearly with sputtering time in this time range.

3.3 Hydrogenation system and experimental procedures

Hydrogen is supplied from the porous substructure (often termed permeate-) side of the membrane which is mounted skin side up in a stainless steel filter holder (47 mm, model XX4404700, Millipore Corp., Billerica, MA). The partial pressure of hydrogen is the driving force for diffusional mass transfer through the skin layer (see Figure 2e). The hydrostatic pressure on the oil side is held above the hydrostatic pressure of the hydrogen to prevent blow-out of the unsupported oil side of the membrane. No gaseous hydrogen will be able to enter the oil in form of bubbles even if membrane defects or pinholes are present since the hydrostatic oil pressure exceeds that of the hydrogen. On the other hand, hydrogen will permeate the membrane skin to be consumed by the hydrogenation reaction after emerging from the oil side surface of the membrane skin. Hydrogen consumption by hydrogenation will maintain the partial pressure driving force across the skin for hydrogen permeation. If the reaction were to reach completion, the hydrogen partial pressure on the two faces of the membrane would eventually equilibrate and no further transport would occur.

A gear pump circulates the hot oil and pressure gauges are present on the hydrogen and oil sides of the membrane. Before the start of the experiment the Pt catalyst on the membrane skin was reduced using hydrogen at 60°C for 15 hours with the permeate side open to the atmosphere. After reduction about 13.7 g of soybean oil was added to the reactor system and the system was purged with nitrogen. The oil was then heated to the reaction temperature and circulated at about 25 grams/min across the Pt sputtered skin side of the membrane. Oil side pressure was always 60 psig using a blanket of ultra high purity (UHP) nitrogen on the oil reservoir. UHP hydrogen was supplied from the porous substructure side of the membrane at 50 psig, and the reaction temperature was maintained at 70°C. Soybean oil samples were taken at regular intervals and analyzed using gas chromatography. A small hydrogen bleed stream was established from the hydrogen (substructure) side of the membrane to prevent accumulation of nitrogen gas permeating from the oil side through the membrane.

3.4 Oil analysis

Oil samples (about 0.1-0.14 grams) were converted to their corresponding fatty acid methyl esters (FAMEs, alternate method in AOCS official method Ce 2-66 [29]). FAMEs thus obtained were analyzed by gas chromatography (GC, 100m CP-Sil 88 column, Hewlett-Packard 6890 series gas chromatograph). AOCS official method Ce 1h-05 was followed for the analysis of fatty acids (Injection port and column 250°C and 181°C, respectively, He carrier gas 1 ml/min, split ratio 1:100).

The extent of hydrogenation of vegetable oil is customarily represented by its Iodine Value (IV) which is the mass of iodine in grams that is consumed under standard conditions by 100 grams of a lipid [30]. The iodine value of the oils was calculated from the compositional analysis (above) by [31]:

$$IV = (\%C_{16:1} \times 0.9502) + (\%C_{18:1} \times 0.8598) + (\%C_{18:2} \times 1.7315) + (\%C_{18:3} \times 2.6152) \quad (1)$$

4 Results and Discussion

4.1 Membrane characterization

4.1.1 Physical characterization of the membrane surface

The morphology of the membrane surface after Pt sputter deposition was studied using atomic force microscopy (AFM). Figure 4 shows the AFM of the native polymer membrane skin and after Pt sputter deposition for 3, 6, and 9 s at 25°C, 100 mTorr air, and 45 mA (note the differences in Z-axis scale from 10 to 250 to 400 nm). Images were analyzed using SPIP software (Image Metrology, Denmark) to calculate the roughness and height of these features on the surface. The native polymer membrane surface is smooth with an average roughness of about 1 nm. Image analysis indicates crests and troughs with a height of up to 5 nanometers and lateral dimensions of about 30-40 nm. These features may be the result of the asymmetric membrane fabrication process. Manual casting can certainly not guarantee a constant speed of the casting knife over the polymer solution and this may well introduce thickness differences such as the "waves" in Figure 4.

After Pt sputter deposition for 3 s uniformly sized features (likely Pt metal) are seen throughout the membrane surface. The features grow in height from 131 nm at 3 s to 340 nm at 6 s Pt sputtering time. Another prominent feature seen after 3 s and 6 s Pt sputtering is the presence of ripples with lateral dimensions of about 30 nm. A rippled topography after sputtering has been observed by others [32; 33]. These ripples may be caused by geometrical effects of atoms deposited on sloped surfaces (see wave-like surface features of the native polymer membrane) through intricate mechanisms [34]. After 9 s sputtering these features become less

prominent and a smoother surface is seen. The average roughness decreases from 69 nm to 27 nm from 6 s to 9 s sputtering. This change in topography may indicate the formation of a more continuous Pt film due to coalescence of small Pt islands (see below).

A thin layer (< 100 nm) of PEI was spin coated on a TEM grid (2000 mesh copper grid, Electron Microscopy Sciences, Hatfield, PA) followed by sputtering under the same conditions as used for the AFM images. This was done to approximate the surface sputtering of the membranes while allowing TEM's to be taken. Figure 5 shows the surface of the polymer film sputtered with Pt for 3, 6, and 9 s, respectively. The dark grey to black Pt islands appear to grow and coalesce with sputtering time. Table 1 gives the properties of the sputtered surface as calculated using the image analysis software ImageJ [35]. As the sputtering time is increased from 3 to 6 s the Pt loading increases from 0.9 to 1.7 $\mu\text{g cm}^{-2}$, the surface area covered by Pt increases from 24 area% to 30 area%, the size of the islands increases from about 4 to about 10 nm, and the island density decreases from 5 to 2 islands per 100 nm^2 . At 9 s sputtering a network of large interconnected islands with little exposed membrane area is apparent. The Pt loading at this stage is 3.4 $\mu\text{g cm}^{-2}$ with about 72 area% of the polymer surface covered with Pt.

Figure 5 seems to indicate growth of Pt islands according to the Volmer-Weber mechanism [36]. In this mechanism during the first growth stage, metal nucleation occurs and metal clusters grow in diameter and there is an increase in the metal islands density. These features are consistent with the 3 s sputtering seen on Figure 5a. As growth proceeds, islands coalesce and enlarge and there is a decrease in island density (Figure 5b). Finally the islands increase in size by branching with other meandering islands until a percolation network of Pt forms [36] as is seen for 9 s (Figure 5c).

The membranes used for hydrogenation experiments were sputtered with Pt under the same conditions and sputtering times as above. We attempt below to rationalize hydrogenation results by drawing on the morphological information presented here and the single gas permeation measurements to characterize membranes before and after sputtering.

4.1.2 Degree of selective skin perfection

The asymmetric membranes evaluated in this study had a range of skin thicknesses and different degrees of skin perfection. The mainly size selective α_{H_2/N_2} determined by dividing single gas fluxes at 50 psig and room temperature was used as a stringent quality criterion. A perfect membrane skin would be indicated by an α_{H_2/N_2} of about 181 (as measured on a thick polymer film at 25 °C [26; 27]). The effective average skin thickness of perfect membrane skins can then be calculated from the known permeability coefficients of PEI films with known thickness. Defects in the polymer skin (transport not by solution-diffusion) will deteriorate α_{H_2/N_2} very rapidly. α_{H_2/N_2} between 181 (thick PEI film) and 3.7 (Knudsen selectivity of pores with a size below the mean free path of gas molecules) indicate that the gas is permeating through the membrane via some combination of solution-diffusion in the dense membrane skin and via permeation through defects with small pore sizes which still will likely prevent oil intrusion into the substructure. α_{H_2/N_2} greater than 181 for sputtered membranes could indicate either that a fraction of the hydrogen is permeating through the metal layer (which has a low permeation rate at this temperature, but an infinite α_{H_2/N_2}) or that the membrane skin polymer has been modified (perhaps densified) by the sputtering process, or a combination of the above.

While membrane skin perfection requirements are very important for gas separation membranes this is less so for the process presented here. Oil intrusion into the membrane and hydrogen bubbling into the oil can be prevented even if α_{H_2/N_2} is less than the intrinsic value

since some Knudsen-diffusion level defects will not cause bubbling or oil intrusion while they will certainly reduce the high intrinsic $\alpha_{\text{H}_2/\text{N}_2}$ significantly.

The influence of the hydrogen delivery mode judged by $\alpha_{\text{H}_2/\text{N}_2}$ of the membranes on the reaction rates and catalytic selectivities was evaluated. While $\alpha_{\text{H}_2/\text{N}_2}$ was in the range of 4 to 220, in no case was oil permeation into the membrane support or through the membrane observed.

If polymeric membranes with minor skin layer defects could be successfully employed in this application, they would be cheaper and easier to manufacture than corresponding membranes with perfectly defect-free skins.

Detection of defects in the sub-micron thick skin of macroscopic areas (several cm^2) of integral-asymmetric membranes on the scale of Knudsen-diffusion type pores is very difficult by direct means. TEM, SEM, and AFM analyses can only scan very small areas. The defects may be few and the skin is inseparably connected to the porous sub-structure that contains the bulk of the polymer. Gas molecules however can serve as very sensitive skin morphology "probes" since the high selectivity $\alpha_{\text{H}_2/\text{N}_2}$ of glassy polymers like PEI is easily destroyed by even a few Knudsen diffusion-scale defects. Therefore, we will attempt below to rationalize the membrane morphology and impact of skin defects based on known physical properties of PEI and Pt, and the measured $\alpha_{\text{H}_2/\text{N}_2}$. It must be acknowledged that gas permeation measurements are certainly only circumstantial evidence of structure and morphology, but they are nonetheless quite sensitive and non-destructive, and are very useful in the absence of other methods to characterize the fine structure of ultrathin layers of a thin film "soft" material bonded to a bulky substructure of the same material.

4.1.3 Effect of Plasma Sputtering on Polymeric Membranes

The possible change in membrane properties (H_2 flux and α_{H_2/N_2}) due to surface modification by ion bombardment in addition to the metal deposition complicates tracking the effect of sputtering. Depending on the conditions employed (ion-energy, composition of ions, ion energy, polymer material, etc.), plasmas are reported to remove adsorbed surface materials/contaminants, etch the polymer, cross-link polymer chains, chemically modify the surface of the polymer, or even create new functional groups on the polymer surface [37; 38; 39]. The processes that lead to these modifications on the polymer surface are known to be highly complex and can not be exhaustively discussed here [39; 40; 41; 42; 43].

Sputtering only modifies the surface (up to about 2 nm depth) without significantly affecting the bulk properties of the material [40]. Therefore, we do not expect additional defects to result from the sputtering process.

Integral asymmetric PEI membranes were processed in the sputtering setup without a metal target to isolate effects on the polymer skin. Figure 6 shows the change in H_2 flux and α_{H_2/N_2} after processing the membrane in the sputterer without any target at 25°C, 100 mTorr air, and 45 mA. The pre-processing α_{H_2/N_2} values indicate that all samples had defects but likely on the order of Knudsen-diffusion type pores. Most of the membranes showed a decrease in selectivity as high as 60% with perhaps a minor increase or no change in hydrogen flux. Ion bombardment can lead to chemical modification, densification of the polymer surface and ablation of the polymer. The chemical modification and densification of the surface layer can lead to a decrease in α_{H_2/N_2} since the leak flux (not impacted by the sputtering plasma) becomes more prominent versus the "selective" flux through the defect-free and now densified areas of the polymer skin.

This may also lead to the observed minor overall decrease in hydrogen flux. However, etching of the polymer surface may result in an increase in the membrane flux.

Probing the membranes by gas permeation does not deliver first-hand evidence but one may surmise that the impact of the plasma in the sputtering process (no metal deposited) seems consistent with effects reported in the literature (densification causing increased ideal gas selectivity but lower flux, ablation increasing the flux through decreasing the skin thickness, unchanged flux though small defects). The sputtering process itself certainly does not cause major changes in the gas transport properties as far as impacting the hydrogenation process is concerned.

4.1.4 Effect of Metal Sputtering on Polymeric Membranes

For the hydrogenation experiments integral-asymmetric PEI membranes were sputter deposited with Pt. Figure 7 shows the percentage reduction in hydrogen flux as a function of virgin membrane α_{H_2/N_2} after Pt sputtering for 3, 6, and 9 s at 25°C, 100 mTorr air pressure, and 45 mA.

A wide variation in the reduction of hydrogen flux after sputtering is evident (0 to 90% flux reduction) even for membranes sputtered for the same amount of time and having similar virgin membrane α_{H_2/N_2} . The factors impacting the gas transport property changes of membranes by metal sputtering can be grouped as follows:

- Flux increase, no selectivity change: plasma ablation of polymer from the non-metal coated areas of the skin

- Flux decrease, selectivity increase: plugging of defects by metal deposition, coverage of polymer with low-permeability/high H₂ selectivity metal, densification/cross linking of polymer via plasma

4.2 *Hydrogenation results*

Table 2 gives the properties of the integral-asymmetric PEI membranes before and after Pt sputtering that were used for hydrogenation experiments. These membranes were selected to evaluate the effect of membrane properties (H₂ flux, and the form of hydrogen supplied) and catalyst loading on the hydrogenation rate, the cis-trans isomerization, and the hydrogenated product composition.

It is important to keep in mind that the single gas hydrogen flux measurements of membranes do not represent the hydrogen flux under hydrogenation conditions. The driving force for single gas measurements of membranes is well defined and constant. However, the driving force during a hydrogenation experiment can change significantly due to perhaps even local buildup of dissolved hydrogen in the oil if hydrogen consumption via hydrogenation cannot keep pace with the hydrogen supplied. The single gas flux measurements nonetheless indicate a "ceiling" for hydrogen transport and can be used to compare membranes with each other, especially in regard to defects.

4.2.1 Effect of membrane flux and selectivity

The hydrogen flux of the membrane controls the maximum rate at which hydrogen can permeate through the membrane during a hydrogenation run. Using membranes with higher hydrogen flux is expected to increase the hydrogenation rate until the catalytic process becomes limiting. The ideal gas selectivity $\alpha_{\text{H}_2/\text{N}_2}$ of a membrane indicates how hydrogen is supplied to the membrane surface. A high selectivity membrane will result in a more uniform supply of

hydrogen across the membrane surface by solution-diffusion through the skin layer while a low selectivity membrane may indicate a portion of hydrogen being supplied through defects and concentrated at relatively few locations on the membrane surface. This hydrogen may or may not contribute effectively towards hydrogenation depending on the distribution of catalyst in the vicinity of the hydrogen source. It should be kept in mind, however, that no hydrogen bubbling can occur since the hydrostatic pressure of the oil exceeds that of the gaseous hydrogen.

In general, hydrogenation rates increase with hydrogen flux of the membrane and then level off. Figure 8 shows the hydrogenation rate (represented as iodine value IV hr⁻¹) with membranes having different hydrogen flux and $\alpha_{\text{H}_2/\text{N}_2}$. In an attempt to try to understand the factors influencing the variability in hydrogenation rate within the data set, we will explore the behavior of a few subsets of the data.

4.2.1.1 High catalyst loading

For membranes with high catalyst loading (3.4 $\mu\text{g Pt cm}^{-2}$), there is an increase in hydrogenation rate with increasing membrane flux and the selectivity of the membrane appears to have only a minor influence on the hydrogenation rate. The hydrogenation rate increased from 1.2 IV hr⁻¹ for a membrane with a hydrogen flux of 0.8 GPU ($\alpha_{\text{H}_2/\text{N}_2}=84$) to 7.4 IV hr⁻¹ for a membrane with hydrogen flux of 10 GPU ($\alpha_{\text{H}_2/\text{N}_2}=5$). This increase in the hydrogenation rate with increasing membrane flux indicates that the hydrogenation rate is limited by the supply of hydrogen through the membrane. Despite this apparent possible hydrogen "starvation" of the catalyst, lower TFA formation as compared to slurry reactors was observed [5].

For a catalyst loading of 3.4 $\mu\text{g cm}^{-2}$, about 70 % of the membrane area is covered with Pt. Thus, the reduction in hydrogen flux is expected to be close to 70% for an essentially defect-free membrane and assuming no significant effect of plasma ion-bombardment on the exposed

polymer surface. However, the presence of defects complicates the impact of metal sputtering on gas transport rates beyond the simple relation to the metal-covered area. A hydrogen flux reduction lower than 70% despite 70% metal area coverage is possible if the distribution of Pt on the membrane surface is such that defects are unaffected by Pt sputtering. This also means that for these cases relatively more of the gas transport after sputtering is through the defects. This can also affect the hydrogenation rate as is seen in Figure 8. Some membranes show lower hydrogenation rates than expected. The membrane with a hydrogen flux of 10 GPU ($\alpha_{\text{H}_2/\text{N}_2}=107$) and the membrane with a hydrogen flux of 23 GPU ($\alpha_{\text{H}_2/\text{N}_2}=120$) both produced hydrogenation rates of about 4.8 IV hr^{-1} , less than might have been expected from the trend of the other data. The membranes that produced unexpectedly low hydrogenation rates also exhibited lower reduction in hydrogen flux after sputtering (refer to Figure 7) which may indicate gas transport through defects. Only a 40% reduction in hydrogen flux after Pt sputtering is observed for the membrane with a final hydrogen flux of 10 GPU ($\alpha_{\text{H}_2/\text{N}_2}=107$), and almost no reduction in hydrogen flux by sputtering is observed for the membrane with a final hydrogen flux of 23 GPU ($\alpha_{\text{H}_2/\text{N}_2}=120$), as compared to close to 90% reduction in hydrogen flux for some other membranes (refer to Figure 7). High hydrogen availability in only certain regions where defects are present can not increase the overall hydrogenation rate proportionally since the process becomes limited by the available catalyst, rather than the hydrogen availability. If all hydrogen was for the sake of argument available in only one location on the membrane surface then most of the catalyst would be likely starved and a low hydrogenation rate would result.

4.2.1.2 Low catalyst loading

For membranes with low catalyst loading ($0.9 \mu\text{g cm}^{-2}$), a moderate increase in hydrogenation rate was obtained by using defect-free membranes having higher hydrogen fluxes.

The hydrogenation rate increased from 4.2 IV hr⁻¹ for membrane with a flux of 8 GPU ($\alpha_{\text{H}_2/\text{N}_2}=222$) to 4.9 IV hr⁻¹ for a membrane with a hydrogen flux of 15 GPU ($\alpha_{\text{H}_2/\text{N}_2}=201$). However, the membranes sputtered for 3 s with Pt showed a significant decrease in hydrogenation rates when using membranes with low $\alpha_{\text{H}_2/\text{N}_2}$. The hydrogenation rate decreased from 4.2 IV hr⁻¹ to 2.5 IV hr⁻¹ when using a membrane with higher hydrogen flux but a much lower selectivity (12.5 GPU and $\alpha_{\text{H}_2/\text{N}_2}=4$ as compared to 7.5 GPU and $\alpha_{\text{H}_2/\text{N}_2}=222$). Even the membrane with a hydrogen flux of 22 GPU and $\alpha_{\text{H}_2/\text{N}_2}=14$ had a lower hydrogenation rate as compared to membrane with a hydrogen flux of 12.5 GPU and an essentially defect-free membrane skin. This significant drop in hydrogenation rate for low selectivity membranes can be explained by comparing the distribution of catalyst on the membrane surface for 3 s sputtering with the distribution obtained after sputtering for 9 s. Sputtering the membrane for 3 s results in small Pt islands (4 nm) with large distances between them and lower surface coverage (24%) while sputtering for 9 s results in an interconnected network of large Pt islands and higher surface coverage (72%) of the membrane with Pt (refer to Figure 5 and Table 1). A defective membrane sputtered with Pt for 3 s would likely result in a significant amount of hydrogen being supplied through these defects on average farther away from most catalytic sites, due to the distribution of catalyst as obtained after sputtering for 3 s. This would result in reduced hydrogen availability at catalytic sites and lead to lower hydrogenation rates as is seen in Figure 8.

In the range studied, the hydrogen flux of the membrane as determined by single gas permeation measurements appeared to have a minor influence on the formation of TFA. Figure 9 compares the TFA formed at an IV of 95 for membranes with different flux and catalyst loadings. For membranes sputtered for 3 s, TFA formation at an IV of 95 was 3.5 wt% for membrane with a hydrogen flux of 15 GPU ($\alpha_{\text{H}_2/\text{N}_2}=201$) and 4.3 wt% for a membrane with a

hydrogen flux of 8 GPU ($\alpha_{H_2/N_2}=222$). For membranes sputtered for 9 s, TFA formation at an IV of 95 was in the range of 2.6-2.8 wt% irrespective of the flux of the membrane.

4.2.2 Effect of catalyst loading for membranes with similar hydrogen transport properties

For membranes with similar hydrogen flux after sputtering, a lower catalyst loading resulted in increased TFA formation at similar hydrogenation levels (refer to Figure 9). A membrane with a hydrogen flux of 8 GPU and catalyst loading $0.9 \mu\text{g cm}^{-2}$ produced 4.3 wt% TFA as compared to 2.6 wt% TFA produced by a membrane with a hydrogen flux of 6 GPU and catalyst loading of $3.4 \mu\text{g cm}^{-2}$ (sputtering time 9 s). This trend of decreased TFA formation with increased catalyst loading is opposed to what is observed in slurry systems where an increase in applied catalyst produces higher TFAs as it results in hydrogen starvation at the surface of the catalyst [4]. However, for catalytic membranes studied here, an increase in catalyst loading from $0.9 \mu\text{g cm}^{-2}$ to $3.4 \mu\text{g cm}^{-2}$, results in a significantly different physical catalyst morphology on the surface of the membrane. Small discrete Pt metal clusters are obtained at $0.9 \mu\text{g cm}^{-2}$, while $3.4 \mu\text{g cm}^{-2}$ results in large interconnected network of islands. When membranes having similar hydrogen flux are used, the catalyst distribution obtained at higher catalyst loadings ($3.4 \mu\text{g cm}^{-2}$) result in higher probability that the hydrogen will be usable by the catalyst thereby producing lower TFAs.

A decrease in TFA formation due to high concentration of hydrogen at the catalyst surface is also generally accompanied by an increase in the amount of fully saturated oil produced [4]. Figure 10 shows the amount of TFA and saturates formed at an IV of 95 for membranes having different catalyst loading. With the increase in catalyst loading from $0.9 \mu\text{g cm}^{-2}$ to $3.4 \mu\text{g cm}^{-2}$, the amount of TFA decreased from 4.6wt% to 2.6 wt%, with an increase in C18:0 saturates from 13 wt% to 19 wt%. The high amount of saturates obtained with membranes having high catalyst

loadings suggests a trade-off between low TFA formation and higher amount of saturates during hydrogenation by having higher hydrogen concentrations at the catalyst surface, as reported in other studies[44], [4].

4.2.3 Effect of membrane properties and catalyst loading on product composition

For the same catalyst and process conditions, the product composition at similar hydrogenation levels will vary depending on the concentration of hydrogen at the surface of the catalyst. The hydrogenation reaction is more selective if the concentration of hydrogen at the surface of the catalyst is low [45]. Figure 11 shows how catalyst loadings can have an effect on the composition of the hydrogenated product. Linolenic acid (C18:3) hydrogenates at the same rate for both the cases. However, the composition profile for all other components varies. Higher amounts of saturates (C18:0), and linoleic acid (C18:2), and lower amounts of oleic acid (C18:1) at similar hydrogenation levels, are produced by using membranes with higher catalyst loadings and a slightly higher hydrogen flux. This may be due to high hydrogen concentration obtained at higher catalyst loading ($3.4 \mu\text{g cm}^{-2}$) as discussed above.

5 Process comparison and outlook

A base case of 100 metric tons of soybean oil to be hydrogenated per day from IV 130 to IV 90 will be assumed. This will stoichiometrically require about 3.7 mol of hydrogen atoms per second. The approach using electrochemical generation of hydrogen [21] will be compared to our approach since both can be performed under conditions compatible with existing facilities and both approaches significantly reduce TFA.

The electrochemical process will require about 270 m^2 of electrochemical reactor area configured as plate and frame cells as suggested in the publication (based on 90% current efficiency and 135 mA/cm^2). About 6.7 kg catalyst will be needed. This can perhaps be reduced

by about 10% by using one anode per two cathodes in a cathode-anode-cathode stack design. The electrochemical process will consume electricity worth about 0.2 cents per kg of soybean oil hydrogenated (0.0678 \$/kWh, per U.S. EIA, April 09) which compared to the raw oil cost is not significant. An electrochemical process will require auxiliary equipment such as rectifiers and control systems to supply over 360,000 A DC current at low voltage.

The metal-decorated membrane approach will require about 2,700 m² membrane area with a total of about 0.09 kg of Pt (~\$3,600). This is based on the 9 s Pt sputtered membranes and about 5 hours to hydrogenate about 13.8 g of oil from IV 130 to 90, using 17.3 cm² of membrane area. A preferred configuration would be outside-skin hollow fibers spun from a glassy polymer like PEI or polysulfone. Metal deposition on various fibers is well established on the industrial scale for optical fibers and many other applications. Gas permeation hollow fibers and modules have been industrially used for many years for processes such as hydrogen separation from gas mixtures or nitrogen production from air. With the relatively high packing density of hollow fiber modules one can envision a module bank of perhaps a hundred to a few hundred 40 inch by 8 inch hollow fiber modules as sufficient to satisfy the above base case. Existing facilities could also gain incremental capacity by adding membrane modules in a bypass to their hydrogenation systems since pressures and temperatures are compatible. No auxiliary equipment besides oil pumping, gas manifolding, and pressure control is needed. Existing facilities are already familiar with these requirements.

The operating costs for both systems seem reasonable considering a much superior product will be made, and since existing hydrogen is assumed to be used. The catalyst costs appear to be lower for the metal-decorated phase inversion membrane system proposed here. The electrochemical system will require significant numbers of relatively costly and complex plate-

and-frame systems while the metal-decorated membranes rely on existing hollow fiber spinning, and module technology, augmented by metal vapor deposition or sputtering on the outside of the fibers. The simplicity of operating the hollow fiber modules compared to introducing an electrochemical system to the soybean oil industry may be an issue to consider. Module replacement also seems perhaps simplified and less expensive with hollow fiber modules compared to electrochemical fuel cells.

6 Conclusion

This study investigated the use of metal decorated integral-asymmetric polymer membranes for partial hydrogenation of soybean oil as an alternative to traditional slurry reactor systems and with the goal to significantly lower the undesirable trans fat content of the traditional hydrogenated product. Hydrogen was supplied directly at or near the skin surface of a Pt-sputtered integral-asymmetric polymeric membrane by pressurizing the porous substructure of the membrane with hydrogen. The oil flows past the Pt sputtered side of the membrane. Dissolved hydrogen and the liquid phase (soybean oil) come in direct contact with each other at the catalyst surface. This approach minimizes the gas-liquid mass-transfer limitations that are often experienced in three phase systems when using traditional slurry reactors. The level of TFA produced in the membrane reactor was very low (2.6-4.6 wt% at Iodine Value of 95). The system is compatible with existing hydrogenation facilities as far as temperature and pressures are concerned. Since the catalyst is immobilized on the membrane, no catalyst recovery is required, and a small amount of catalyst is sufficient. Membranes having different hydrogen flux, H_2/N_2 selectivity and catalyst loadings were tested for hydrogenation runs to evaluate the properties that have a significant impact on the process. The results show that hydrogen flux and

H₂/N₂ selectivity of the composite membrane have only a minor influence on TFA formation. In the range studied, TFA formation decreased with an increase in the catalyst loading.

***Acknowledgements** The project was supported by the National Research Initiative of the USDA Cooperative State Research, Education and Extension Service, grant number 2005-35503-153*

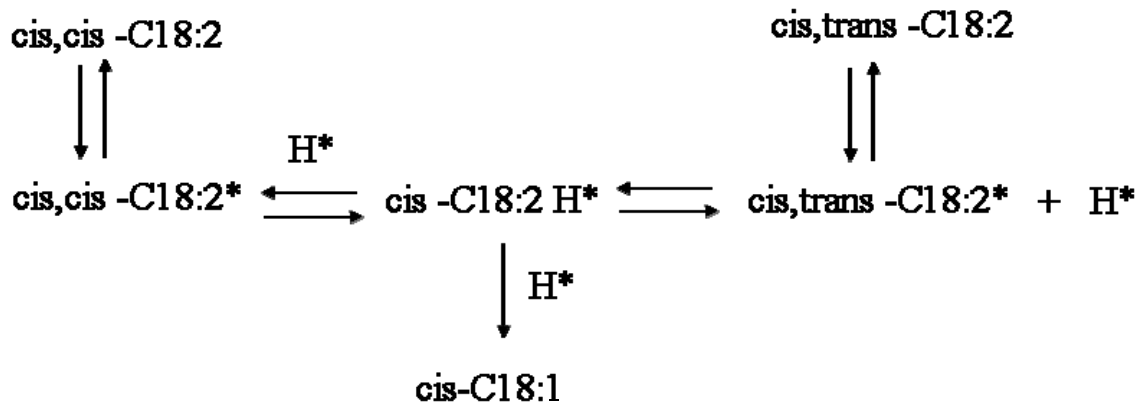


Figure 1: The hydrogenation of Linoleic fatty acid (C18:2) to Oleic acid (C18:1) (* indicates species adsorbed on the catalyst surface).

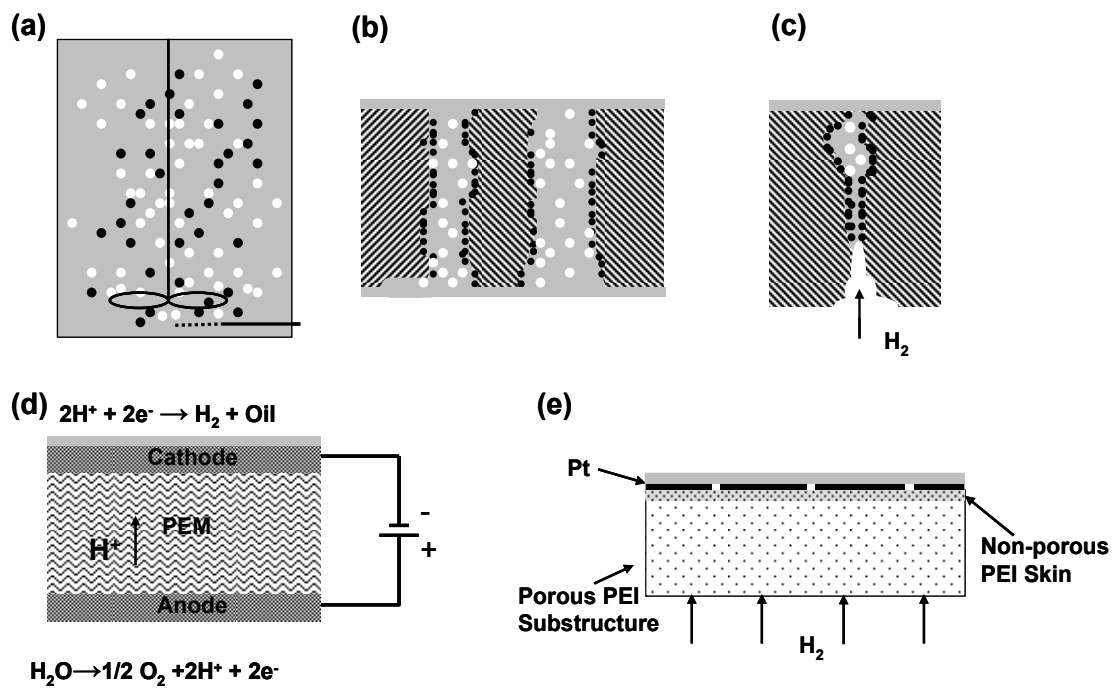


Figure 2: Hydrogenation of vegetable oils: a) traditional slurry reactor b) flow-through contactor mode c) diffuser mode with liquid on the catalyst side d) Hydrogenation combined with water electrolysis to supply hydrogen e) metal decorated integral-symmetric polymer membrane (this work).

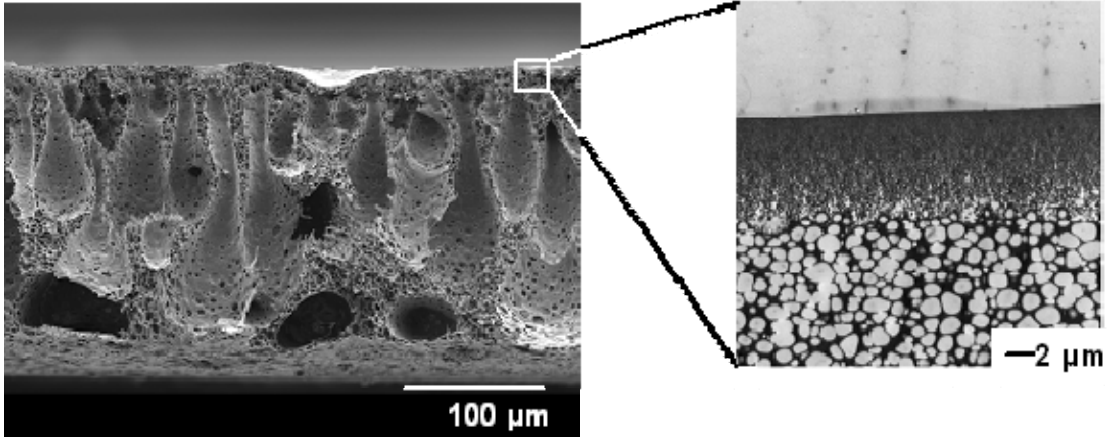
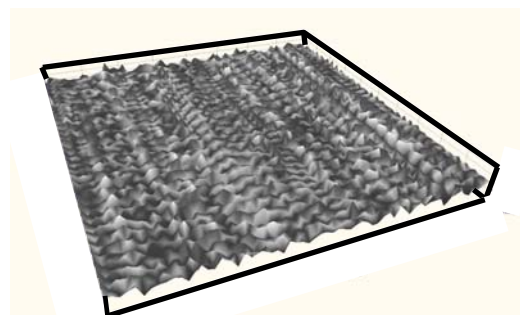


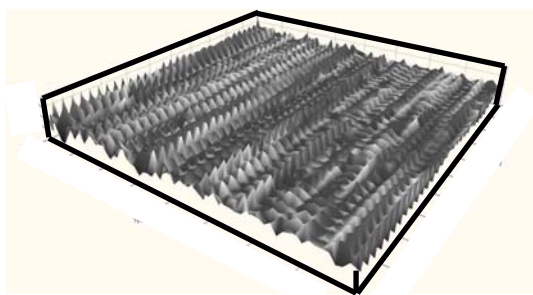
Figure 3: Cross-section of integral asymmetric PEI membrane showing the porous substructure and the dense skin. Left, SEM of the substructure with the skin at the top of the image. Right: TEM image of the skin showing the transition from a highly porous substructure to an essentially defect-free, dense skin.



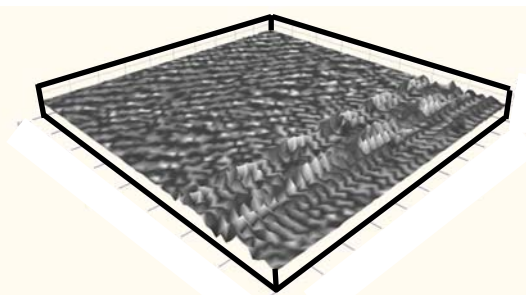
Native polymer (100x100x10 nm)



3s Pt sputtering (200x200x250 nm)



6s Pt sputtering (200x200x400 nm)



9s Pt sputtering (200x200x400 nm)

Figure 4: AFM of native polymer surface and after sputtering with Pt. The native membrane surface is flat. Uniformly sized features appear on the membrane surface after 3 s Pt sputtering. These features grow in height after 6 s sputtering and appear flattened after 9 s Pt sputtering, as the valleys between the peaks are gradually filled.

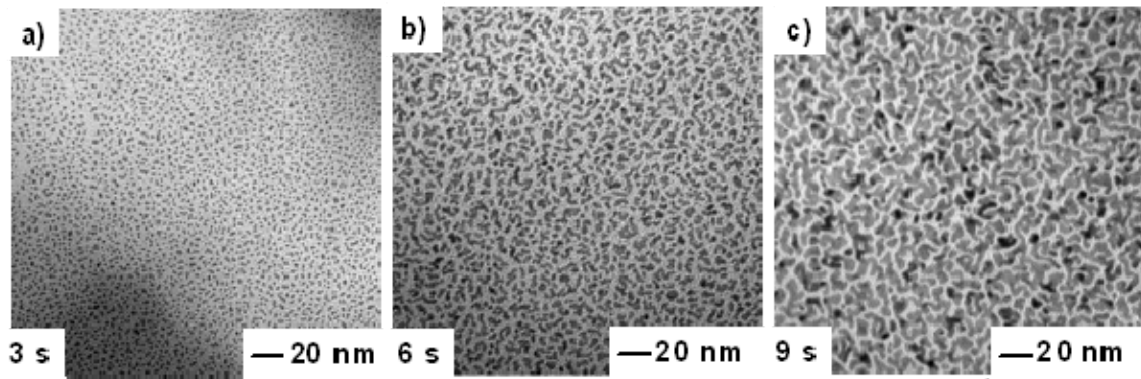


Figure 5: TEMs of the surface of PEI films sputtered with Pt. Isolated Pt metal islands formed after 3 s sputtering and increase in size after 6 s sputtering and, growing to an interconnected network of islands after 9 s sputtering. Further sputter leads to grain coarsening.

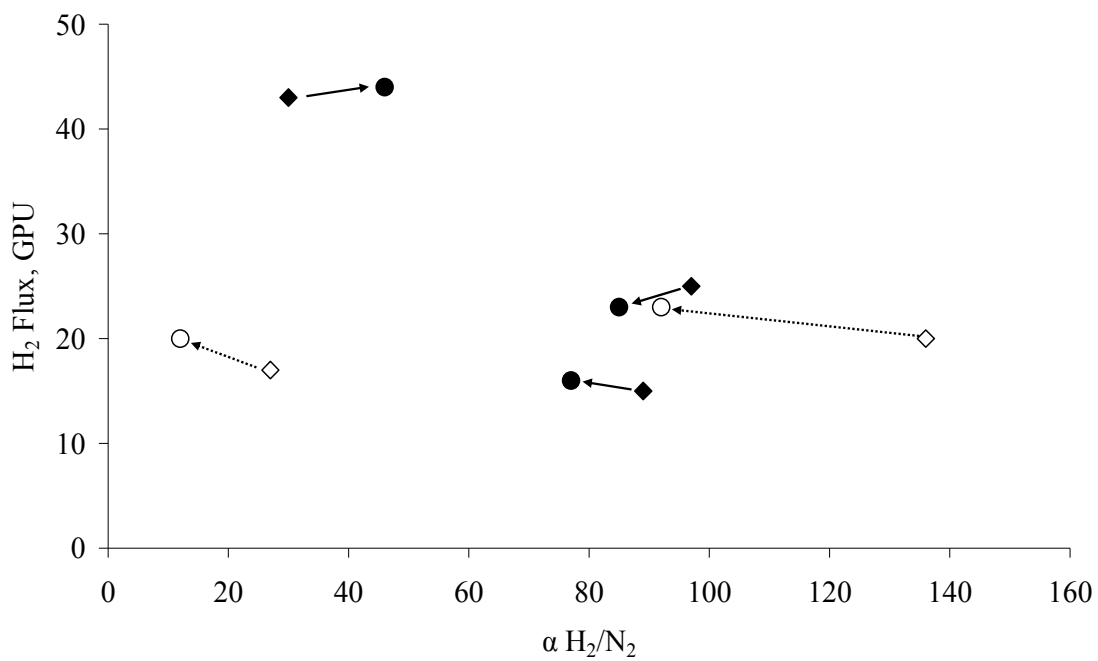


Figure 6: Effect of the sputter process in the absence of a metal target on the properties of integral asymmetric PEI membranes (100 mTorr air, 25°C, 45 mA). A decrease in selectivity is observed for most membranes with a moderate increase in hydrogen flux. From the limited data presented, no distinguishing patterns can be observed for the treatment at 3 s versus 9 s.

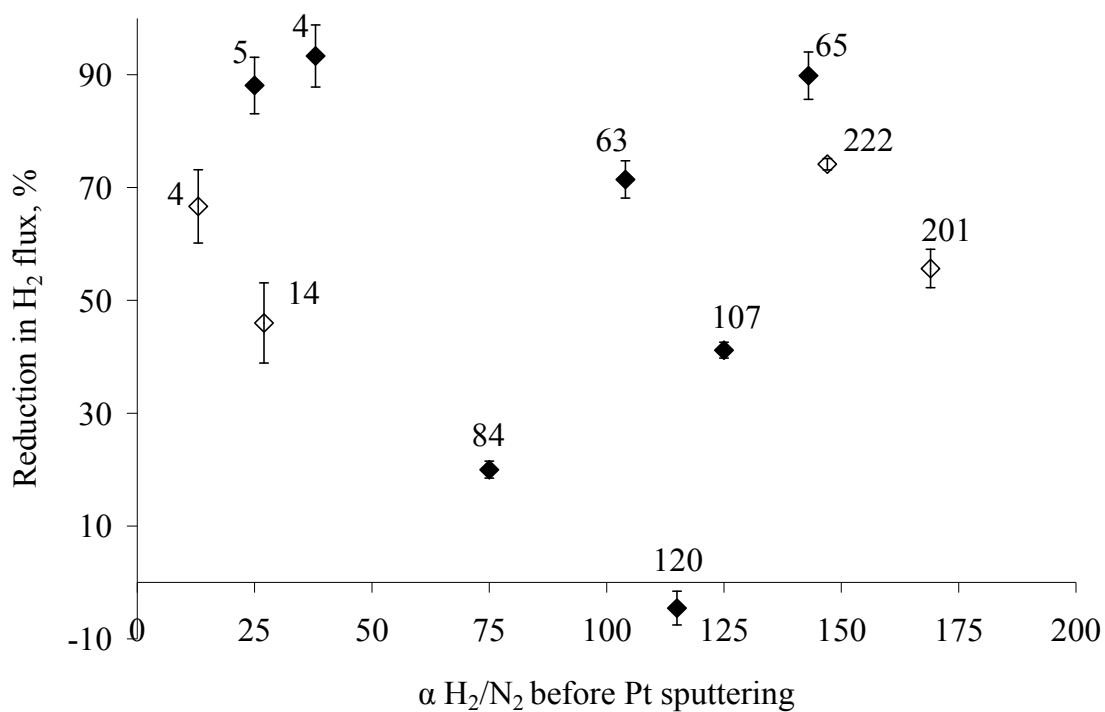


Figure 7: Effect of Pt metal sputtering on hydrogen flux and selectivity for 3 s (\diamond), and 9 s (\blacklozenge) Pt sputtering. Labels indicate $\alpha_{\text{H}_2/\text{N}_2}$ after sputtering. The figure shows a wide variation in the reduction of hydrogen flux through sputtering with Pt. (error bars represent the standard deviation of multiple analyses)

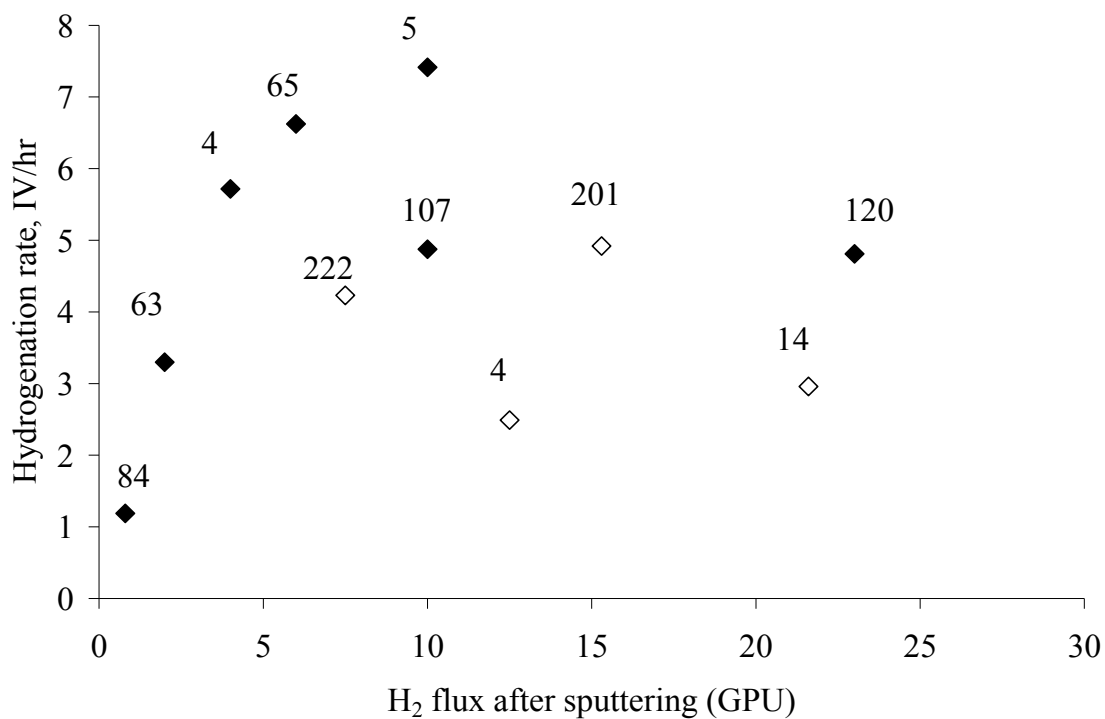


Figure 8: Effect of hydrogen flux and $\alpha_{\text{H}_2/\text{N}_2}$ (both measured after sputtering) on the hydrogenation rate, Pt sputtering for 3 seconds (\diamond), and 9 seconds (\blacklozenge). The labels indicate $\alpha_{\text{H}_2/\text{N}_2}$ after sputtering. Reaction conditions: 70 °C, hydrogen pressure 50 psig.

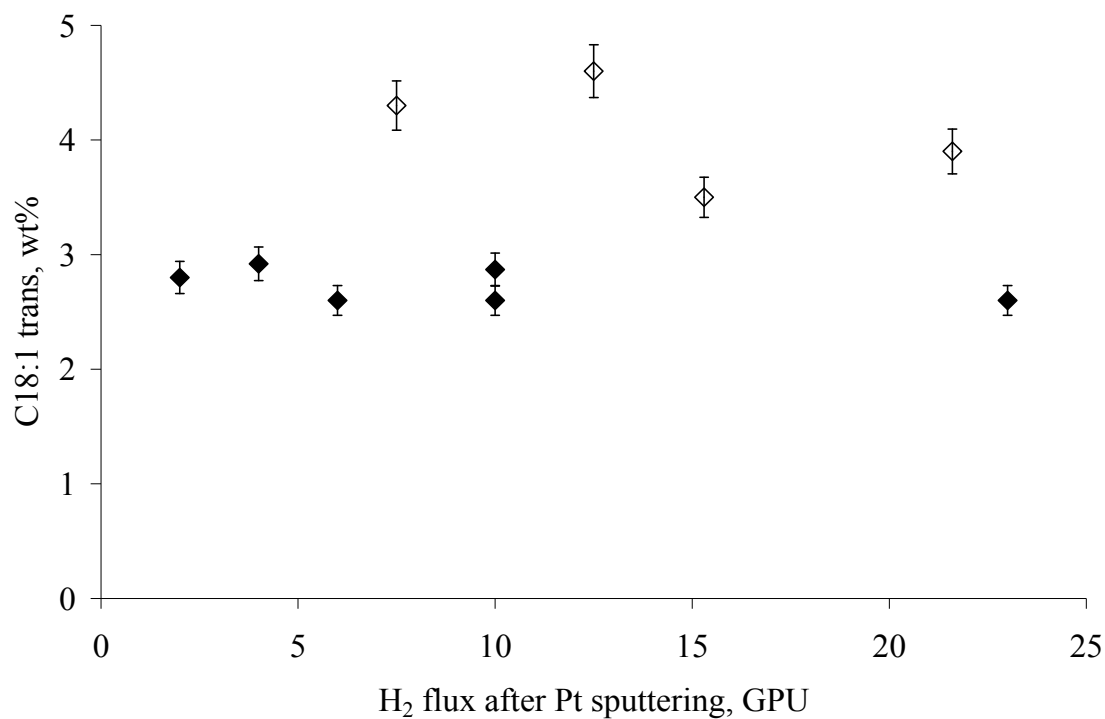


Figure 9: Effect of hydrogen flux of the membrane (measured after sputtering) on TFA formation (at IV 95), Pt sputtering for 3 seconds (\diamond), and 9 seconds (\blacklozenge). Reaction conditions 70°C, hydrogen pressure 50 psig (error bars represent the standard deviation of multiple analyses).

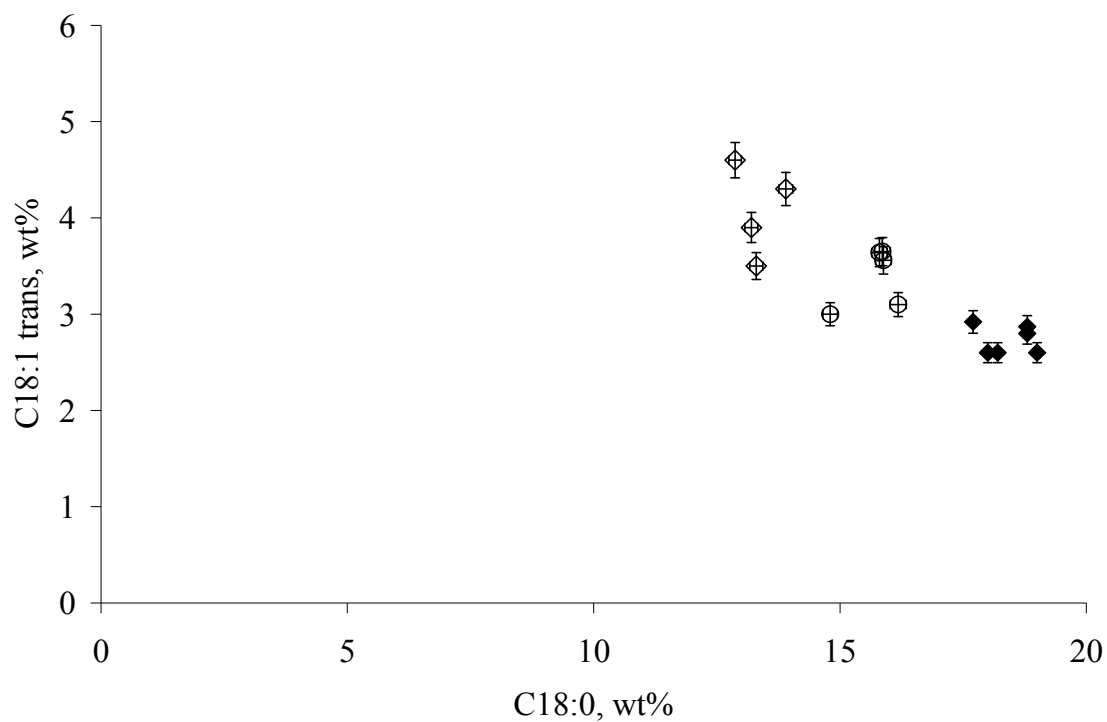


Figure 10: Effect of sputtering time on TFA and saturates (at IV 95) for 3 seconds (\diamond), 6 seconds (\circ), and 9 seconds (\blacklozenge) Pt sputtering. Reaction conditions 70°C, hydrogen pressure 50 psig. A decrease in TFA formation and increase in C18:0 saturates is seen with increase in catalyst loading. (error bars represent the standard deviation of multiple analyses)

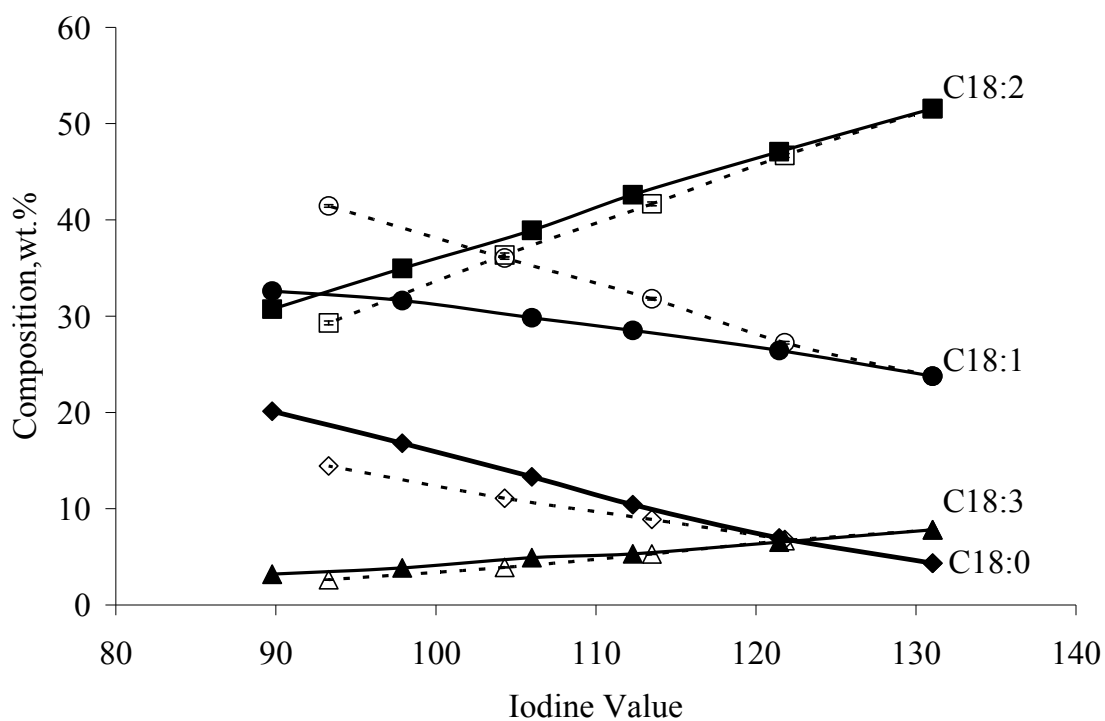


Figure 11: Effect of membrane properties on the composition of soybean oil during hydrogenation:

solid lines: catalyst loading $0.9 \mu\text{g cm}^{-2}$, hydrogen flux = 8 GPU

dashed lines: catalyst loading $3.4 \mu\text{g cm}^{-2}$, hydrogen flux = 10 GPU

(Reaction conditions 70°C , hydrogen pressure 50 psig)

Table 1: Metal deposition and membrane area coverage for Pt sputtering of the skin side of integral-asymmetric PEI gas separation membranes.

Sputtering time [s]	Pt loading, [$\mu\text{g cm}^{-2}$]	Approx. average metal island diameter [nm]	Number of metal islands per area [$\#/100 \text{ nm}^2$]	Metal coverage [area %]
3	0.9	4	5	24
6	1.9	10	2	30
9	3.4	-	Interconnected network of islands	72

Table 2: Properties of integral-asymmetric PEI membranes used in the experiment, before and after sputtering with Pt. (25°C, 50 psig feed pressure)

H₂ flux [GPU]	Ideal gas selectivity α_{H_2/N_2}	H₂ flux [GPU]	Ideal gas selectivity α_{H_2/N_2}
Before sputtering		After sputtering	
<i>3 seconds sputtering</i>			
35	169	15	201
29	147	7.5	222
40	27	22	14
38	13	12.5	4
<i>6 seconds sputtering</i>			
24	136	15	196
21	125	6	183
11	120	4	140
17	20	14	19
77	17	19	5
<i>9 seconds sputtering</i>			
59	143	6	65
17	125	10	107
22	115	23	120
7	104	2	63
1*	75	0.8*	84
60	38	4	4
84	25	10	5

*Membrane with 4 GPU flux operated at 10 psig hydrogen pressure (equivalent flux=0.8 GPU).

References

- [1]U.S. Census. Bureau, Current industrial reports. M311K, Fats and oils production, consumption, and stocks. in: U.S. Census Bureau, (Ed.), 2007.
- [2]A. Dejonge, J.W.E. Coenen, and C. Okkerse, Selective Hydrogenation of Linolenate Groups in Soya-Bean Oil. *Nature* 206 (1965) 573-574.
- [3]A. Musavi, M. Cizmeci, A. Tekin, and M. Kayahan, Effects of hydrogenation parameters on trans isomer formation, selectivity and melting properties of fat. *European Journal of Lipid Science and Technology* 110 (2008) 254-260.
- [4]A.J. Dijkstra, Revisiting the formation of trans isomers during partial hydrogenation of triacylglycerol oils. *European Journal of Lipid Science and Technology* 108 (2006) 249-264.
- [5]D. Singh, P.H. Pfromm, and M.E. Rezac, Partial Hydrogenation of Soybean Oil with Minimal Trans Fat Production Using a Pt-Decorated Polymeric Membrane Reactor. *Journal of American Oil Chemists' Society* 86 (2009) 93-101.
- [6]R. Mateos, M. Trujillo, M.C. Perez-Camino, W. Moreda, and A. Cert, Relationships between oxidative stability, triacylglycerol composition, and antioxidant content in olive oil matrices. *Journal of Agricultural and Food Chemistry* 53 (2005) 5766-5771.
- [7]J.E. Hunter, Dietary levels of trans-fatty acids: basis for health concerns and industry efforts to limit use. *Nutrition Research* 22 (2005) 499-513.
- [8]C.M. Oomen, M.C. Ocke, E.J.M. Feskens, M.A.J. van Erp-Baart, F.J. Kok, and D. Kromhout, Association between trans fatty acid intake and 10-year risk of coronary heart disease in the Zutphen Elderly Study: a prospective population-based study. *Lancet* 357 (2001) 746-751.
- [9]J.W.B. Veldsink, Martin J.; Schoon, Nils-H.; Beenackers, Antonie A. C. M., Heterogeneous hydrogenation of vegetable oils: a literature review. *Catalysis Reviews - Science and Engineering* 39 (1997) 253-318.
- [10]R.J. Grau, A.E. Cassano, and M.A. Baltanas, Catalysts and Network Modeling in Vegetable Oil Hydrogenation Processes. *Catalysis Reviews-Science and Engineering* 30 (1988) 1-48.
- [11]W.E. Farr, Hydrogenation: processing technologies. in: F. Shahidi, (Ed.), *Bailey's Industrial Oil and Fat Products*, John Wiley & Sons, 2005.
- [12]I. Horiuti, and M. Polanyi, Exchange reactions of hydrogen on metallic catalysts. *Trans. Faraday Soc.* 30 (1934) 1164 - 1172.
- [13]B. Fillion, B.I. Morsi, K.R. Heier, and R.M. Machado, Kinetics, gas-liquid mass transfer, and modeling of the soybean oil hydrogenation process. *Industrial & Engineering Chemistry Research* 41 (2002) 697-709.
- [14]R.J. Grau, A.E. Cassano, and M.A. Baltanas, Solution of a Complex-Reaction Network - the Methyl-Linoleate Catalytic-Hydrogenation. *Chemical Engineering Communications* 58 (1987) 17-36.
- [15]M. Plourde, K. Belkacemi, and J. Arul, Hydrogenation of sunflower oil with novel Pd catalysts supported on structured silica. *Industrial & Engineering Chemistry Research* 43 (2004) 2382-2390.

- [16]G.R. List, W.E. Neff, R.L. Holliday, J.W. King, and R. Holser, Hydrogenation of soybean oil triglycerides: Effect of pressure on selectivity. *Journal of the American Oil Chemists Society* 77 (2000) 311-314.
- [17]P.N. Pintauro, Synthesis of a low-trans content edible oil, non-edible oil, or fatty acid in a solid polymer electrolyte reactor, US Patent No. 6,218,556 B1, 2001.
- [18]C.M. Piqueras, I.O. Costilla, P.G. Belelli, N.J. Castellani, and D.E. Damiani, Pd-gamma Al₂O₃ applied to triglycerides hydrogenation with supercritical propane Experimental and theoretical catalysts characterization. *Applied Catalysis a-General* 347 (2008) 1-10.
- [19]A. Schmidt, and R. Schomacker, Partial hydrogenation of sunflower oil in a membrane reactor. *Journal of Molecular Catalysis a-Chemical* 271 (2007) 192-199.
- [20]J.W. Veldsink, Selective hydrogenation of sunflower seed oil in a three-phase catalytic membrane reactor. *Journal of the American Oil Chemists Society* 78 (2001) 443-446.
- [21]P.N. Pintauro, M.P. Gil, K. Warner, G. List, and W. Neff, Electrochemical hydrogenation of soybean oil with hydrogen gas. *Industrial & Engineering Chemistry Research* 44 (2005) 6188-6195.
- [22]W.D. An, J.K. Hong, P.N. Pintauro, K. Warner, and W. Neff, The electrochemical hydrogenation of edible oils in a solid polymer electrolyte reactor. II. Hydrogenation selectivity studies. *Journal of the American Oil Chemists Society* 76 (1999) 215-222.
- [23]K. Mondal, and S.B. Lalvani, Electrochemical hydrogenation of canola oil using a hydrogen transfer agent. *Journal of the American Oil Chemists Society* 80 (2003) 1135-1141.
- [24]K.V. Peinemann, K. Fink, and P. Witt, Asymmetric Polyetherimide Membrane for Helium Separation. *Journal of Membrane Science* 27 (1986) 215-216.
- [25]K.C. Obrien, W.J. Koros, T.A. Barbari, and E.S. Sanders, A New Technique for the Measurement of Multicomponent Gas-Transport through Polymeric Films. *Journal of Membrane Science* 29 (1986) 229-238.
- [26]T.A. Barbari, W.J. Koros, and D.R. Paul, Polymeric Membranes Based on Bisphenol-a for Gas Separations. *Journal of Membrane Science* 42 (1989) 69-86.
- [27]M.E. Rezac, and B. Schoberl, Transport and thermal properties of poly(ether imide) acetylene-terminated monomer blends. *Journal of Membrane Science* 156 (1999) 211-222.
- [28]S.A. Steward, Review of hydrogen isotope permeability through materials, Lawrence Livermore National Laboratory, 1983.
- [29]AOCS, Preparation of methyl esters of fatty acids, Official methods and recommended practices of the AOCS, American Oil Chemists' Society, Champaign, Ill., 1998, pp. Ce 2-66.
- [30]W.W. Nawar, Chemistry. in: Y.H. Hui, (Ed.), *Bailey's Industrial Oil & Fat Products* John Wiley & Sons, Inc., 1996.
- [31]S. Petursson, Clarification and expansion of formulas in AOCS recommended practice Cd 1c-85 for the calculation of iodine value from FA composition. *Journal of the American Oil Chemists Society* 79 (2002) 737-738.

- [32]S. Balaji, P.V. Satyam, V. Lakshminarayanan, and S. Mohan, Influence of secondary ion bombardment on the composition, structure and surface properties of platinum thin films. *Nuclear Instruments & Methods in Physics Research Section B-Beam Interactions with Materials and Atoms* 217 (2004) 423-428.
- [33]E.R. Scott, H.S. White, and D.J. McClure, Scanning Tunneling Microscopy of Platinum Films on Mica - Evolution of Topography and Crystallinity during Film Growth. *Journal of Physical Chemistry* 93 (1989) 5249-5253.
- [34]D.G. Cahill, Morphological instabilities in thin-film growth and etching. *Journal of Vacuum Science & Technology A* 21 (2003) S110-S116.
- [35]T.J. Collins, ImageJ for microscopy. *Biotechniques* 43 (2007) 25-30.
- [36]P. Andreazza, C. Andreazza-Vignolle, J.P. Rozenbaum, A.L. Thomann, and P. Brault, Nucleation and initial growth of platinum islands by plasma sputter deposition. *Surface & Coatings Technology* 151 (2002) 122-127.
- [37]D.M. Coates, and S.L. Kaplan, Modification of polymeric surfaces with plasmas. *Mrs Bulletin* 21 (1996) 43-45.
- [38]R. Foerch, and D.H. Hunter, Remote Nitrogen Plasma Treatment of Polymers - Polyethylene, Nylon 6,6, Poly(Ethylene Vinyl Alcohol), and Poly(Ethylene-Terephthalate). *Journal of Polymer Science Part a-Polymer Chemistry* 30 (1992) 279-286.
- [39]J.J. Vegh, D. Nest, D.B. Graves, R. Bruce, S. Engelmann, T. Kwon, R.J. Phaneuf, G.S. Oehrlein, B.K. Long, and C.G. Willson, Molecular dynamics simulations of near-surface modification of polystyrene: Bombardment with Ar⁺ and Ar⁺/radical chemistries. *Journal of Applied Physics* 104 (2008) 034308.
- [40]M.C. Coen, R. Lehmann, P. Groening, and L. Schlapbach, Modification of the micro- and nanotopography of several polymers by plasma treatments. *Applied Surface Science* 207 (2003) 276-286.
- [41]A. Delcorte, P. Bertrand, and B.J. Garrison, Collision cascade and sputtering process in a polymer. *Journal of Physical Chemistry B* 105 (2001) 9474-9486.
- [42]A. Delcorte, and B.J. Garrison, Kiloelectronvolt argon-induced molecular desorption from a bulk polystyrene solid. *Journal of Physical Chemistry B* 108 (2004) 15652-15661.
- [43]P.N. Maya, U. von Toussaint, and C. Hopf, Synergistic erosion process of hydrocarbon films: a molecular dynamics study. *New Journal of Physics* 10 (2008) Article # 023002.
- [44]C.A. Piqueras, G. Tonetto, S. Bottini, and D.E. Damiani, Sunflower oil hydrogenation on Pt catalysts: Comparison between conventional process and homogeneous phase operation using supercritical propane. *Catalysis Today* 133 (2008) 836-841.
- [45]H.B.W. Patterson, Hydrogenation of fats and oils, Applied Science Publishers Ltd., 1983.